Imaging of the Vulnerable Plaque: Biological Targeting of Inflammation in Atherosclerosis using Fluorescent-labelled Dual-ligand Microparticles of Iron Oxide and MRI

Joyce M.S. Chan, MBBS, PhD, MRCS,[a,b,c] Claudia Monaco, MD, PhD, FESC,[d] Marzena Wylezinska-Arridge, PhD,[e] Jordi L. Tremoleda DVM, PhD,[f] Jennifer. E. Cole, PhD,[d] Michael Goddard, BSc,[d] S.H. Cheung, MPhil,[a] Kishore K. Bhakoo, PhD,[c] and Richard G.J. Gibbs, MD, FRCS [b]

[a] Department of Surgery, Prince of Wales Hospital, The Chinese University of Hong Kong, Hong Kong.

[b] Regional Vascular Unit, St Mary's Hospital, Imperial College Healthcare NHS Trust, Imperial College London, United Kingdom.

[c] Laboratory of Molecular Imaging, Singapore Bioimaging Consortium, Agency for Science, Technology and Research (A*STAR), Singapore.

[d] Kennedy Institute of Rheumatology, Nuffield Department of Orthopaedics, Rheumatology and Musculoskeletal Sciences, University of Oxford, United Kingdom.

[e] Neuroradiological Academic Unit, UCL Institute of Neurology, University College London, London, United Kingdom.

[f] MRC-Clinical Sciences Centre, Imperial College London; Centre for Trauma Sciences, Queen Mary University of London, London, United Kingdom.

Corresponding author:

Joyce M. S. Chan

Address: Department of Surgery, Prince of Wales Hospital, The Chinese University of Hong Kong, Hong Kong.

Tel: (852) 5591 8082

Fax: (852) 2637 7947

Email: joycechan@me.com

Word count: 3,475 words

Abbreviations and Acronyms

$ApoE^{-/-}$	= Apolipoprotein-E deficient
BSA	= bovine serum albumin
CAS	= carotid artery stenting
CEA	= carotid endarterectomy
DMEM	= Dulbecco's Modified Eagle's Medium
DT-MPIO	= dual-targeted microparticles of iron oxide
EC	= endothelial cells
ECL	= enhanced chemiluminescence
HSS	= high shear stress
ICA	= internal carotid artery
IDA	= iron deficiency anaemia
LCCA	= left common carotid artery
LSS	= low shear stress
MIP-3	= macrophage inflammatory protein-3
MRA	= magnetic resonance angiography
MRI	= magnetic resonance imaging
OCT	= optimal cutting temperature
OSS	= oscillatory shear stress
PBS	= phosphate-buffered saline
PFA	= paraformaldehyde
RCCA	= right common carotid artery
ROI	= region of interest
SMC	= smooth muscle cells
SNR	= signal-to-noise ratio
SPIO	= superparamagnetic iron oxide
TBS	= Tris buffered saline
TNFα	= tumour necrosis factor-α
TOF	= time of flight
USPIO	= ultrasmall superparamagnetic particles of iron oxide
VCAM-1	= vascular cell adhesion molecule-1

CENTRAL PICTURE

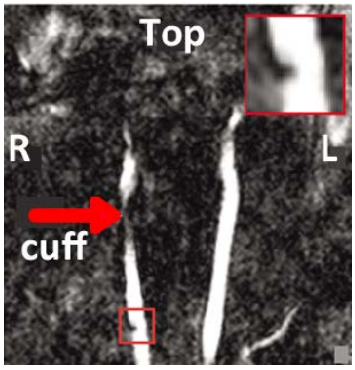

Dual-targeted MPIO-enhanced MRI can identify vulnerable carotid plaques from stable ones.

CENTRAL MESSAGE

Dual-targeted MPIO constitute a novel imaging tool for quantitative assessment of inflammation in atherosclerosis. Translation into clinical arena will improve risk stratification in carotid disease.

PERSPECTIVE STATEMENT

Identification of patients with high-risk asymptomatic carotid plaques remains an elusive but essential step in stroke prevention. Currently there is no clinical imaging tool to assess intraplaque inflammation. Dual-targeted MPIO constitute a novel imaging tool for characterization of plaque vulnerability and inflammation at molecular level, permitting accurate risk stratification in carotid disease.

ABSTRACT

Objectives: Identification of patients with high-risk asymptomatic carotid plaques remains an elusive but essential step in stroke prevention. Inflammation is a key process in plaque destabilization, a prelude to clinical sequelae. There are currently no clinical imaging tools to assess the inflammatory activity within plaques. This study aims at characterizing inflammation in atherosclerosis using dual-targeted microparticles of iron oxide (DT-MPIO) as an MRI probe.

Methods: DT-MPIO were used to detect and characterize inflammatory markers, VCAM-1 and P-selectin, on i) TNFα-treated cells by immunocytochemistry; ii) aortic root plaques of Apolipoprotein-E deficient (*ApoE*$^{-/-}$) mice by in vivo MRI. Furthermore, *ApoE*$^{-/-}$ mice with focal carotid plaques of different phenotypes were developed by means of peri-arterial cuff placement to allow in vivo molecular MRI using these probes. The association between biomarkers and MR signal in different contrast groups was assessed longitudinally in these models.

Results: Immunocytochemistry confirmed specificity and efficacy of DT-MPIO to VCAM-1 and P-selectin. Using this in vivo molecular MRI strategy, we demonstrated; i) DT-MPIO-induced MR signal tracked with VCAM-1 (r=0.69, P=0.014), P-selectin (r=0.65, P=0.022), and macrophage content (r=0.59, P=0.045) within aortic root plaques; ii) high-risk inflamed plaques were distinguished from non-inflamed ones in the murine carotid artery within a practical clinical imaging time frame.

Conclusions: These molecular MRI probes constitute a novel imaging tool for in vivo characterization of plaque vulnerability and inflammatory activity in atherosclerosis.

Further development and translation into the clinical arena will facilitate more accurate risk stratification in carotid atherosclerotic disease in the future. (246 words)

INTRODUCTION

Carotid endarterectomy (CEA) and carotid artery stenting (CAS) for symptomatic internal carotid artery (ICA) atherosclerotic lesions are well-recognized interventions in stroke prevention. The case for intervention in asymptomatic lesions has become more controversial with the development of better medical preventative treatment, and with an annual stroke risk of 1-2%[1] for asymptomatic threshold disease it is more difficult to justify surgery or stenting. Nonetheless, asymptomatic benign atherosclerotic lesions do go on to become unstable and lead to thromboembolic stroke, but currently there is no reliable imaging tool to identify these vulnerable lesions.

Promising non-invasive imaging techniques are currently being developed to interrogate plaque vulnerability in vivo.[2] Molecular magnetic resonance imaging (MRI) has the distinct advantage of providing precise soft tissue and functional information in vivo by acquiring different contrast weightings, enabling co-registration of molecular with anatomical information into a single imaging modality.[3,4] Superparamagnetic iron oxide (SPIO) particles have become favored MR contrast agents because of a known biocompatibility profile, significant contrast effect and ease of production.[4] Iron oxide particles increase sensitivity and facilitate diagnosis by shortening transverse T2 and T2* relaxation times, resulting in hypointense signals that appear darker on T2- and T2*-weighted MR images ('negative' contrast).[4]

Molecular MRI comprises 'passive' and 'active' imaging strategies. Ultrasmall superparamagnetic particles of iron oxide (USPIO) have been used as passive contrast agents to identify plaque macrophages as surrogate markers of plaque inflammation in assessing atherosclerosis in human and animal models.[5,6] 'Active' molecular imaging

involves direct reporting of specific molecular events, which mandates the use of a specific targeting system. Target specificity of contrast agents can be achieved through conjugation of a variety of targeting ligands, such as monoclonal antibodies, antibody fragments, peptides, to functional groups on the surface of iron-oxide particles.[7]

Inflammation is a key driver of plaque instability. Macrophages play a vital role in plaque destabilization, converting chronic stable lesions into acute unstable ones with the potential for thromboembolism. Monocyte recruitment into vascular tissues is promoted by the overexpression of adhesion molecules, such as vascular cell adhesion molecule-1 (VCAM-1; CD106), and P-selectin (CD62P), on the activated endothelium.[8,9] Furthermore, VCAM-1 is also expressed on activated smooth muscle cells (SMC) and macrophages, both of which are major plaque constituents.[10] Exploiting the abundance and critical functions of these inducible adhesion molecules, we previously developed a dual-targeting strategy directed at VCAM-1 and selectin on human carotid plaque tissues using antibody-conjugated SPIO particles as MRI probes for visualizing inflammation.[11] Using these molecular MRI probes, the potentially high-risk inflamed plaques have been identified and differentiated from the non-inflamed ones within the asymptomatic plaque population by ex vivo MRI.[11] Recently, microparticles of iron oxide (MPIO) was used in imaging endovascular targets.[12] Compared with USPIO and SPIO, larger MPIO has a greater iron oxide content, hence can generate significant MR contrast effect to enable detection of vascular targets in vivo.

In this study, we have developed fluorescent-labelled dual-ligand microparticles of iron oxide (MPIO) against VCAM-1 and P-selectin to act as a contrast agent in order to render adhesion molecules MR visible. Adhesion molecules were detected and characterized in

in vitro and in vivo *ApoE*$^{-/-}$ mouse model. The extent to which dual-targeted MPIO (DT-MPIO) induced MR signal tracks adhesion molecules and inflammation by in vivo MRI is evaluated. Further, we sought to determine whether asymptomatic carotid plaques could be distinguished based on the degree of inflammation exhibited using these MRI probes in an in vivo model.

MATERIALS AND METHODS

See Supplementary Materials.

RESULTS

Specificity and Efficacy of Dual-MPIO

The three key cell-types that constituent a plaque, were used in the present study, including mouse endothelial cells (C166), smooth muscle cells (MOVAS) and macrophages (RAW 264.7). These cell-types were stimulated by TNF-α to induce expression of VCAM-1 and/or P-selectin (Figure 1, A). Activated endothelial cells (EC) expressed both markers (Figure 1, A, top) while activated smooth muscle cells (SMC) and activated macrophages expressed only VCAM-1 (Figure 1, A, middle and bottom). Activated EC, SMC and macrophages, expressing VCAM-1 and/or P-selectin, were targeted by fluorescent-labelled DT-MPIO (Figure 1, A, right panel). MPIO conjugated with non-specific IgG was used as control. Compared to single-ligand targeted MPIO, dual-conjugated MPIOs demonstrated more efficient targeting for activated EC due to the synergistic relationship between VCAM-1 and P-selectin (Figure 1, B). To further examine the specificity of DT-MPIO, the stimulated cells were pre-blocked with either of

the single antibody [VCAM-1 antibody (V-Ab) or P-selectin antibody (P-Ab)], or both antibodies (PV-Ab) together. DT-MPIO binding was significantly reduced in cells pre-blocked with either of the single antibody, and was almost absent when both target sites were blocked by PV-Ab (Figure 1, C). These data corroborated with the high specificity of DT-MPIO to the target sites of VCAM-1 and P-selectin.

To investigate the efficacy of DT-MPIO binding, the three cell lines were stimulated with different doses of TNFα to induce varying degrees of inflammation. We observed that the higher the dose of TNFα used, the greater the degree of inflammation as indicated by the higher level of VCAM-1 and/or P-selectin expression, hence a greater amount of DT-MPIO binding to the cells (Figure 2, A, left panel). DT-MPIO binding not only increased with greater degree of inflammation, but also significantly correlated with the cell expression of VCAM-1 and P-selectin (Figure 2, A, right panels). To further examine the binding efficiency, the stimulated cells were incubated with DT-MPIO over a period up to 4 hours. The cell-bound DT-MPIO was detected as early as 15 minutes following stimulation, with optimal uptake between 1 to 2 hours (Figure 2, B).

Cytotoxicity and Biodistribution of Dual-MPIO

An MTT assay was performed to evaluate the cytotoxicity of DT-MPIO in the three cell lines. Cell viability remained high in all cell lines after 24 hours incubation with DT-MPIO at doses ranging from 0 to 2 mg/mL. We observed no significant cytotoxicity at the concentration used for the subsequent in vivo study (1 mg/ml, equivalent to 5 mg Fe/kg) (Figure 3, A). We next examined the in vivo biodistribution of DT-MPIO from 30 minutes to 72 hours after intravenous administration (Figure 3, B). MPIO was quantified

as mass of magnetic particles per mg of tissue. MPIO uptake occurred in all tissues as early as 30 minutes after injection with minimal retention by lung tissue. The rapid uptake of MPIO by spleen and liver continued up to 48 hours as expected. No ill effects or symptoms were observed up to 72 hours after MPIO administration.

Determination of Optimal Imaging Time Window by Histology, Ex Vivo In Situ MRI and In Vivo MRI

Firstly, we performed in vivo administration of DT-MPIO which was allowed to circulate in *ApoE*$^{-/-}$ mice up to 2 hours prior to histology. Immunostaining on serial aortic root sections revealed DT-MPIO targeting the inflamed plaque as early as 30 minutes (Figure 4, A), persisting up to 2 hours (Figure 4, B). DT-MPIO targeting was specific to inflamed plaque lesions, without binding to disease free aortic root (Figure 4, A). No binding of IgG-MPIO to inflamed lesions was observed for up to 2 hours.

Secondly, we examined the feasibility of detection of aortic root lesions in *ApoE*$^{-/-}$mice by ex vivo in situ MRI following in vivo administration of DT-MPIO (Figure 4, C). The study also demonstrated the rapid binding of DT-MPIO to atherosclerotic plaques as early as 30 minutes under in vivo condition. Discrete circular hypointensity signal areas on the luminal side of the aortic root were observed in the DT-MPIO group. We speculate that this is due to the 'blooming effect' caused by the magnetic field distortion of MPIO. This was confirmed by the presence of iron using Perls' stain on aortic root lesions in the matching sections. In contrast, no discrete hypointensity signal was detected in IgG-1-MPIO group, which was confirmed by minimal Perls' stain on the aortic root lesions (Figure 4, C).

Thirdly, in vivo serial MRI of aortic root was performed from 20 minutes post-injection up to 2 hours. In the DT-MPIO group, new hypointensity signal was visualized from 30 to 45 minutes post-injection, and persisted for the entire 2-hour imaging period (Figure 5, A). The dark signal appeared to be diffuse, extending between the peri-luminal and peri-adventitial regions of the aortic root in the post-contrast images (Figure 5, A). The hypointensity effect was due to MPIO binding to plaques, which was confirmed by histology (Figure 5, B). In the IgG-MPIO group, a negligible degree of homogeneous hypointensity was seen in the post-contrast image (Figure 5, B). This was supported by minimal binding of the non-specific IgG-MPIO in the aortic root lesions (Figure 5, B).

Relationship between Markers of Plaque Inflammation and the Magnitude of Change in SNR

The sample characteristics, mean signal change and amount of iron binding in the plaques in the two contrast groups are summarized in Figure 6A and 6B. Signal change was significantly higher in the mice given DT-MPIO (27.95±10.24) compared to the IgG-MPIO group (5.58±2.87, $P<0.001$). Iron was also higher in the DT-MPIO (7.80±1.37) compared to the IgG-MPIO group (3.66±2.24, $P<0.001$). The DT-MPIO induced MR signal also quantitatively tracked with VCAM-1, P-selectin and macrophage burden within plaque lesions [VCAM-1: ($r=0.69$, $P=0.014$); P-selectin: ($r=0.65$, $P=0.022$); macrophages: ($r=0.59$, $P=0.045$)]. In contrast, the IgG-MPIO induced MR signal did not reflect or track these markers of inflammation within plaque lesions ($r= -0.43$, $P=0.337$; $r=0.19$, $P=0.702$ and $r= -0.11$, $P=0.819$, respectively) (Figure 6, C, D and E). There were also interactions between biomarkers and contrast groups, with an increase in VCAM-1

[β(se)=0.88(0.37), *P*=0.030] and P-selectin [β(se)=1.04(0.48), *P*=0.049] associated with a significantly greater increase in signal change in DT-MPIO group than IgG-MPIO.

Detection and Characterization of Vulnerable Carotid Plaques by In Vivo Magnetic Resonance Angiography (MRA) using Dual-MPIO

A shear stress modifying cuff was utilized to induce plaque lesions of both stable and vulnerable phenotypes along the same carotid artery in an *ApoE*$^{-/-}$ mouse model. In vivo MRA of carotid arteries was subsequently performed to determine whether DT-MPIO can detect vulnerable plaques. In the DT-MPIO group, new areas of discrete dark signal were detected on the luminal side in the low shear stress (LSS) region (upstream or proximal to the cuff) of the right common carotid artery (RCCA) in the post-contrast images of all three planes, i.e. sagittal, coronal and axial (Figure 7, A). By contrast, no new discrete dark signal was seen on the luminal side in 1) high shear stress (HSS) region (within the cuff) or 2) oscillatory shear stress (OSS) region (downstream or distal to the cuff) of RCCA, and 3) throughout the left common carotid artery (LCCA) in the post-contrast images (Figure 7, A).

In control IgG-1-MPIO group, no new discrete dark signal was observed in all regions of RCCA and throughout LCCA in post-contrast images. No ill effect or symptom was observed after cuff placement and administration of iron particles until the end of the scanning session.

Dual-MPIO Selectively Bind to Lesions with Vulnerable Plaque Phenotype but Not to Stable Lesions

Histological analysis confirmed that all animals developed lesions in the RCCA in LSS and OSS regions post-cuff placement (Figure 7, A). However, the lesions had a strikingly different morphology. In the LSS region, the lesions were characterized by a vulnerable plaque phenotype, i.e. high macrophage content, thin layers of smooth muscle cells and collagen in the cap of the lesion. In the OSS region, the lesions were characterized by relatively stable phenotype, i.e. relatively low macrophage content, thicker layers of smooth muscle cells and collagen uniformly distributed in the intima. No atherosclerotic lesion was observed in both the HSS region in RCCA or in the non-treated LCCA.

In the DT-MPIO treated group, the majority of Perls' stain for iron particles was observed in the lesions with a vulnerable phenotype in the LSS region of the RCCA. Minimal Perls' stain was observed in the lesions with a relatively stable phenotype in the OSS region. Absence of Perls' stain was confirmed in the atherosclerosis-spared areas in the HSS region in the RCCA and undisturbed control LCCA (Figure 7, A).

The results suggested that DT-MPIO selectively bound not only to lesions, but also specifically bound to lesions with vulnerable plaque phenotype. Moreover, the results confirmed that the discrete dark signal detected on the post-contrast MRA in the LSS region on the RCCA was attributable to DT-MPIO targeting at the vulnerable plaque lesions in that region (Figure 7, A). The minimal or absent Perls' stain for iron in the histological sections concurred with the absence of discrete dark signal in the matching post-contrast MRA in the following regions: 1) the lesions of relatively stable phenotype in the OSS region, 2) the atherosclerosis-spared areas in the HSS region in the RCCA and 3) the control LCCA (Figure 7, A).

In the control group, no Perls' stain, hence no non-specific IgG-MPIO binding, was observed in all regions. The results concurred with the absence of discrete dark signal throughout both carotid arteries in the matching post-contrast MRA.

To further investigate the differential patterns of MPIO binding in different regions of carotid artery, expressions of VCAM-1, P-selectin and macrophage inflammatory protein-3 (MIP-3) were examined in each region. The mRNA levels of these genes in the LSS region were significantly higher than those in the OSS region, which was in turn, higher than those in the HSS region (Figure 7, B). The results were also consistent with their expressions at protein level as shown in Figure 7C. These data corroborated that DT-MPIO selectively targeted to the vulnerable inflamed plaques in LSS region, where VCAM-1, P-selectin and MIP-3 were highly expressed, as opposed to plaques with relatively stable and less inflamed phenotype in the OSS region.

DISCUSSION

Despite level 1 evidence, there is no consensus on the best management of patients with asymptomatic carotid artery disease.[14] Even if every asymptomatic patient were to be offered carotid interventions, 95% of all strokes would still occur.[15] Furthermore, 94% of all CEA/CAS in asymptomatic patients in the US were ultimately deemed unnecessary, costing US$2 billion annually.[15,16] The annual stroke risk in patients on the best medical treatment within ACAS and ACST is diminishing, challenging the propriety of basing contemporary guidelines on historical data.[14] Yet, a small cohort of asymptomatic patients who bear high-risk plaques will undoubtedly benefit from intervention.[17] The next paradigm is to accurately identify and treat these high-risk individuals specifically,

rather than continuing with a policy of mass intervention, with little benefits for patients in the long run.

Here, we have developed a dual-imaging modality using MRI, fluorescence microscopy and fluorescent-labelled dual-targeted MPIO to target high-risk inflamed plaques. This molecular imaging strategy benefits from swift binding of MPIO and maintenance of steady state at targets, with rapid clearance of unbound particles from the blood pool, to achieve potent and quantifiable contrast effects in vivo.

USPIO have been used in the clinical setting for risk stratification because they predominantly accumulate in macrophages within high-risk lesions.[5] However, their relatively long blood half-life, which increases background contrast effects and the delay between USPIO injection and imaging, may restrict widespread clinical use, particularly in the acute setting. The recommended interval of contrast circulation time in the majority of animal models and human studies was 5 to 7 days,[18,19] and 24 to 36 hours respectively,[20] although the targeted USPIO that have recently been described have shortened this interval to between 8 to 24 hours in animal models.[21,22] Moreover, the plaque macrophage population is involved in constant influx and excursion.[23] In the event of acute thromboembolism such as stroke or myocardial infarction, the delay in imaging may pose a challenge to differentiate whether the signal detected was due to the plaque instability that provokes rupture and symptoms or after-effect of the event.

Compared to nanoscale particles, ligand-conjugated MPIO are potentially better suited for imaging acute inflammatory processes in conditions, such as atherosclerosis[12,24,25] and ischaemic-reperfusion injury.[26] Our study further elucidated the advantages of DT-MPIO in imaging acute clinical events, which are: i) The high iron content of MPIO yields a

substantially greater signal-to-noise ratio per particle, with a contrast effect approximately 50 times their physical size.[12] As demonstrated here, such "blooming effect" of MPIO greatly enhances their sensitivity to achieve in vivo detection of molecular targets. ii) The half-life of our MPIO (1.748 minutes) is significantly shorter than that of nanoparticles. The swift clearance of unbound MPIO from circulation minimizes background blood phase contrast, enhancing target-to-background ratio and plaque visualization. iii) Similar to previous studies,[12,24] the DT-MPIO against VCAM-1 and P-selectin are designed to mimic the rapid binding process of peripheral blood leukocytes to the vessel wall. Here, we have shown the high specificity and synergistically augmented binding of DT-MPIO to VCAM-1 and P-selectin. Owing to the swift antigen-antibody reaction, cellular binding of DT-MPIO occurred within 15 minutes and peaked at 1 to 2 hours. Similarly, under in vivo condition, the DT-MPIO-induced MR signals were evident between 30 minutes to 2 hours post-injection—a practical imaging time frame for acute thromboembolic events. iv) The large surface area of MPIO enables greater loading capacity of antibodies to these particles, thereby increasing the binding efficiency of targeted MPIO to the adhesion molecules. v) Quantitative reporting of local plaque inflammatory status is a prime objective in the risk stratification and characterization of atherosclerotic disease. DT-MPIO-induced MR signal not only reflected the degree of inflammation, but also tracked closely with VCAM-1 and P-selectin expression under both in vitro and in vivo conditions. This concurred with our earlier work that characterized these inflammatory markers on activated endothelial cells[27] and human carotid plaques[11] by MRI using antibody conjugated SPIO. The present results affirm that the MRI combined with the dual-

355 targeted MPIO approach could potentially offer a novel imaging tool for quantitative
356 assessment of inflammation across a range of atherosclerotic lesions complexities in the
357 future. The potent contrast sensitivity, rapid binding and clearance kinetics of DT-MPIO
358 facilitate an evident 'target-to-background' and quantifiable contrast effect within a
359 practical imaging time frame. This distinguishes DT-MPIO as a valuable molecular
360 imaging platform in the context of imaging acute clinical events. If reproduced in humans,
361 these characteristics would be ideal for clinical application.

362 To date, the degree of luminal stenosis alone assessed by conventional angiographic
363 techniques has not been effective in identifying high-risk asymptomatic subgroup
364 patients[14]. Studies have used the peri-arterial collar to induce atherosclerosis in mouse
365 model for molecular MRI. Herein, we further demonstrate that we can use an in vivo
366 molecular MRI strategy to differentiate the heterogeneity (i.e. stable versus unstable
367 lesions) within the asymptomatic plaque population and to identify high-risk vulnerable
368 plaques in the murine carotid artery within a practical imaging time frame. It is also
369 interesting to note that outward remodeling of the carotid artery (Figure 7, A) left the
370 lumen relatively patent, which would mean the high-risk plaques would remain
371 undetected by conventional MRA. However, the high-risk plaques were detected by DT-
372 MPIO-enhanced MRA. The molecular MRI strategy may potentially overcome the
373 limitation of current angiographic techniques by interrogating the inflammatory status
374 within the plaques. The lesions were induced in the carotid artery instead of other
375 vascular beds, moving a step closer to translating this in vivo imaging strategy to patients
376 with carotid atherosclerotic disease.

377 No obvious cytotoxicity or ill effects of the MPIO on the animals was observed. Iron

particles, being biodegradable, have a satisfactory biocompatibility profile.[28,29] Multiple iron particles agents, such as Ferumoxytol, have been clinically approved as an MRI contrast medium or as an iron replacement product for treatment of iron deficiency anaemia (IDA).[29] The biosafety of iron particles via the intravenous route is also witnessed in imaging human carotid atherosclerosis[30] and treatment for IDA in patients with chronic kidney disease,[31] indicating that these products have a reasonable safety profile corresponding to standard toxicological and pharmacological tests.[32]

The dose of MPIO administered in our study was 5 mg iron per kg body weight, which was slightly higher than that used clinically for non-targeted iron contrast agents in human oncological imaging (2.6 mg/kg),[33] but significantly lower than some USPIO doses used experimentally for imaging larger animal models such as rabbits (11–56 mg/kg).[34,35] In this study, a relatively high dose was used to see if the signal attenuation was feasible for detection of atherosclerotic lesions. Further optimization of the dose of MPIO is warranted in future studies. Although this molecular imaging tool has been validated in various stages, we hope to repeat with a larger sample size in large animal model.

With the ongoing CREST-2 and ACTRIS evaluating imaging features in the high-risk asymptomatic cohorts, we hope this molecular MR imaging tool could potentially allow characterization of plaque vulnerability and quantitative imaging of inflammatory activity in atherosclerosis in the future. This facilitates accurate risk stratification of individual patients; identification of the high-risk patient subgroup with unstable inflamed plaque disease, affording the opportunity for early preventive intervention and paving the way for personalized management of carotid artery disease. This work will form the basis for

401 a translational study with direct clinical relevance to patients with cerebrovascular
402 diseases.

Competing interests

The authors declare that they have no competing interests.

Authors' contributions

JMSC wrote the paper, designed and performed experiments; MWA, JLT, JEC and MG designed and performed experiments; SHC performed experiments and data collection; RGJG, CM and KKB supervised the study and the writing of the paper. All authors read and commented on the manuscript.

REFERENCES

1. Nicolaides AN, Kakkos SK, Griffin M, Sabetai M, Dhanjil S, Tegos T, et al. Severity of asymptomatic carotid stenosis and risk of ipsilateral hemispheric ischaemic events: results from the ACSRS study. *Eur J Vasc Endovasc Surg.* 2005;30:275-84.
2. Chan J, Gibbs RGJ. Inflammation imaging in carotid assessment. In: Roger M Greenhalgh eds. 34th Symposium Book Vascular and Endovascular Controversies Update. BIBA Publishing, 2012.
3. Corti R, Fuster V. Imaging of atherosclerosis: magnetic resonance imaging. *Eur Heart J*. 2011;32:1709-19b.
4. Mulder WJM, Jaffer FA, Fayad ZA, Nahrendorf M. Imaging and nanomedicine in inflammatory atherosclerosis. *Sci Transl Med*. 2014;6:239sr1.
5. Tang TY, Howarth SP, Miller SR, Graves MJ, Patterson AJ, U-King-Im JM, et al. The ATHEROMA (Atorvastatin Therapy: Effects on Reduction of Macrophage Activity) Study. Evaluation using ultrasmall superparamagnetic iron oxide-enhanced magnetic resonance imaging in carotid disease. *Am Coll Cardiol*. 2009;53:2039-50.
6. Sigovan M, Boussel L, Sulaiman A, Sappey-Marinier D, Alsaid H, Desbleds-Mansard C, et al. Rapid-clearance iron nanoparticles for inflammation imaging of atherosclerotic plaque: initial experience in animal model. *Radiology*. 2009;252:401-9.
7. Choudhury RP, Fisher EA. Molecular imaging in atherosclerosis, thrombosis, and vascular inflammation. *Arterioscler Thromb Vasc Biol*. 2009;29:983-91.

8. Davies MJ, Gordon JL, Gearing AJ, Pigott R, Woolf N, Katz D, et al. The expression of the adhesion molecules ICAM-1, VCAM-1, PECAM, and E-selectin in human atherosclerosis. *J Pathol*. 1993;171:223-9.

9. Ramos CL, Huo Y, Jung U, Ghosh S, Manka DR, Sarembock IJ, et al. Direct demonstration of P-selectin- and VCAM-1-dependent mononuclear cell rolling in early atherosclerotic lesions of apolipoprotein E deficient mice. *Circ Res*. 1999;84:1237–44.

10. Iiyama K, Hajra L, Iiyama M, Li H, DiChiara M, Medoff BD, et al. Patterns of vascular cell adhesion molecule-1 and intercellular adhesion molecule-1 expression in rabbit and mouse atherosclerotic lesions and at sites predisposed to lesion formation. *Circ Res*. 1999;85:199–207.

11. Chan JMS, Monaco C, Wylezinska-Arridge M, TremoledA JL, Gibbs RGJ. Imaging of the vulnerable carotid plaque: biological targeting of inflammation in atherosclerosis using iron oxide particles and MRI. *Eur J Vasc Endovasc Surg*. 2014;47:462-9.

12. McAteer MA, Schneider JE, Ali ZA, Warrick N, Bursill CA, von zur Muhlen C, et al. Magnetic resonance imaging of endothelial adhesion molecules in mouse atherosclerosis using dual-targeted microparticles of iron oxide. *Arterioscler Thromb Vasc Biol*. 2008;28:77-83.

13. Cheng C, Tempel D, van Haperen R, van der Baan A, Grosveld F, Daemen MJ, et al. Atherosclerotic lesion size and vulnerability are determined by patterns of fluid shear stress. *Circulation*. 2006;113:2744-53.

14. Naylor AR. Time to rethink management strategies in asymptomatic carotid artery disease. *Nat Rev Cardiol*. 2012;9:116–24.
15. Naylor AR. Why is the management of asymptomatic carotid disease so controversial? *Surgeon*. 2015;13:34-43.
16. Naylor AR, Gaines PA, Rothwell PM. Who benefits most from intervention for asymptomatic carotid stenosis: patients or professionals? *Eur J Vasc Endovasc Surg*. 2009;37:625-32.
17. Halliday A, Harrison M, Hayter E, Kong X, Mansfield A, Marro J, et al. 10-year stroke prevention after successful carotid endarterectomy for asymptomatic stenosis (ACST‐1): a multicenter randomised trial. *Lancet*. 2010;376:1074–84.
18. Hyafil F, Laissy JP, Mazighi M, Tchétché D, Louedec L, Adle-Biassette H, et al. Ferumoxtran-10-enhanced MRI of the hypercholesterolemic rabbit aorta: relationship between signal loss and macrophage infiltration. *Arterioscler Thromb Vasc Biol*. 2006;26:176–81.
19. Durand E, Raynaud JS, Bruneval P, Brigger I, Al Haj Zen A, Mandet C, et al. Magnetic resonance imaging of ruptured plaques in the rabbit with ultrasmall superparamagnetic particles of iron oxide. *J Vasc Res*. 2007;44:119–28.
20. Trivedi RA, U-King-Im JM, Graves MJ, Cross JJ, Horsley J, Goddard MJ, et al. In vivo detection of macrophages in human carotid atheroma: temporal dependence of ultrasmall superparamagnetic particles of iron oxide-enhanced MRI. *Stroke*. 2004;35:1631–5.

21. Wen S, Liu DF, Cui Y, Harris SS, Chen YC, Li KC, et al. In vivo MRI detection of carotid atherosclerotic lesions and kidney inflammation in ApoE-deficient mice by using LOX-1 targeted iron nanoparticles. *Nanomedicine*. 2014;10:639-49.
22. Segers FM, den Adel B, Bot I, van der Graaf LM, van der Veer EP, Gonzalez W, et al. Scavenger receptor-AI-targeted iron oxide nanoparticles for in vivo MRI detection of atherosclerotic lesions. *Arterioscler Thromb Vasc Biol*. 2013;33:1812-9.
23. Ley K, Miller YI, Hedrick CC. Monocyte and macrophage dynamics during atherogenesis. *Arterioscler Thromb Vasc Biol*. 2011;31:1506-16.
24. McAteer MA, Mankia K, Ruparelia N, Jefferson A, Nugent HB, Stork LA, et al. A leukocyte-mimetic magnetic resonance imaging contrast agent homes rapidly to activated endothelium and tracks with atherosclerotic lesion macrophage content. *Arterioscler Thromb Vasc Biol*. 2012;32:1427-35.
25. Yan F, Yang W, Li X, Liu H, Nan X, Xie L, et al. Magnetic resonance imaging of atherosclerosis using CD81-targeted microparticles of iron oxide in mice. *Biomed Res Int*. 2015;2015:758616.
26. Akhtar AM, Schneider JE, Chapman SJ, Jefferson A, Digby JE, Mankia K, et al. In vivo quantification of VCAM-1 expression in renal ischemia reperfusion injury using non-invasive magnetic resonance molecular imaging. *PLoS One*. 2010;5:e12800.
27. Chan JMS, Cheung MSH, Gibbs RGJ, Bhakoo KK. MRI detection of endothelial cell inflammation using targeted superparamagnetic particles of iron oxide (SPIO). *Clin Transl Med*. 2016;Accepted.

28. Usman A, Sadat U, Patterson AJ, Tang TY, Varty K, Boyle JR, et al. Use of ultrasmall superparamagnetic iron oxide particles for imaging carotid atherosclerosis. *Nanomedicine (Lond).* 2015;10,3077-87.
29. Jin R, Lin B, Li D, Ai H. Superparamagnetic iron oxide nanoparticles for MR imaging and therapy: design considerations and clinical applications. *Curr Opin Pharmacol*. 2014;18:18–27.
30. Kooi ME, Cappendijk VC, Cleutjens KB, Kessels AG, Kitslaar PJ, Borgers M, et al. Accumulation of ultrasmall superparamagnetic particles of iron oxide in human atherosclerotic plaques can be detected by in vivo magnetic resonance imaging. *Circulation*. 2003;107:2453–8.
31. Singh A, Patel T, Hertel J, Bernardo M, Kausz A, Brenner L. Safety of ferumoxytol in patients with anemia and chronic kidney disease. *Am J Kidney Dis*. 2008;52:907-15.
32. Corot C, Robert P, Idée JM, Port M. Recent advances in iron oxide nanocrystal technology for medical imaging. *Adv Drug Deliv Rev*. 2006;58:1471-1504.
33. Will O, Purkayastha S, Chan C, Athanasiou T, Darzi AW, Gedroyc W, et al. Diagnostic precision of nanoparticle-enhanced MRI for lymph-node metastases: a meta-analysis. *Lancet Oncol*. 2006;7:52-60.
34. Ruehm SG, Corot C, Vogt P, Kolb S, Debatin JF. Magnetic resonance imaging of atherosclerotic plaque with ultrasmall superparamagnetic particles of iron oxide in hyperlipidemic rabbits. *Circulation*. 2001;103:415-22.

35. Schmitz SA, Coupland SE, Gust R, Winterhalter S, Wagner S, Kresse M, et al. Superparamagnetic iron oxide-enhanced MRI of atherosclerotic plaques in Watanabe hereditable hyperlipidemic rabbits. *Invest Radiol*. 2000;35:460-71.

LEGENDS

FIGURE 1. Specificity of Dual-MPIO in TNFα stimulated cells. A, C166 (endothelial cells, EC), MOVAS (smooth muscle cells, SMC) and RAW264.7 (macrophages) were treated with TNFα (10 ng/mL) for 24 hours to induce VCAM-1 and P-selectin expressions. DT-MPIO was then incubated with both TNFα treated and untreated cells. Activated EC, SMC and macrophages with VCAM-1 and/or P-selectin expression (red) were bound by fluorescent-labelled DT-MPIO (green). No green fluorescence signal was detected on activated cells when incubated with IgG-MPIO. B, Stimulated EC were incubated with either single (V-MPIO or P-MPIO), DT-MPIO or control IgG-MPIO. DT-MPIO showed a synergistic relationship between VCAM-1 and P-selectin with a significantly enhanced binding efficiency, compared to either V-MPIO or P-MPIO alone (n = 9). C, Stimulated EC were initially treated with antibody against either VCAM-1 (V-Ab), P-selectin (P-Ab) or both (PV-Ab) to block the target sites on the cells before incubation with DT-MPIO. In the control, stimulated cells were not pre-treated by any antibodies prior to incubation with DT-MPIO. These cells were bound by abundant amount of DT-MPIO as shown in green fluorescence signal. The stimulated cells pretreated by P-Ab had P-selectin target sites blocked, leaving only VCAM-1 to be targeted by the DT-MPIO. Hence, DT-MPIO binding was significantly reduced, demonstrated by the low green fluorescence signal. Likewise, DT-MPIO binding was significantly reduced in cells pretreated by V-Ab. When both target sites were blocked by PV-Ab, minimal DT-MPIO binding was observed (n = 9). Bars show mean ± SEM and * represents $P < 0.05$. Three independent experiments were performed and three images were used as quantification in each independent experiment.

FIGURE 2. Efficacy of Dual-MPIO in TNFα stimulated cells. A, All three cell lines (only EC shown here) were treated with TNFα (0 - 100 ng/mL) for 24 hours to induce varying degree of inflammation. Post incubation with fluorescent-labelled DT-MPIO (green fluorescence) was then performed to assess the area of cell-bound MPIO per cell. Cell-bound MPIO (green fluorescence) increased with degree of inflammation and highly correlated with VCAM-1/P-selectin expression probed with corresponding antibody (red fluorescence) in EC and SMC (n = 9). B, Time-point study of three stimulated cell lines under DT-MPIO incubation. Increased cell-bound MPIO (green fluorescence) with time in EC and SMC but to a lesser degree in macrophages (n = 9). The cell binding of DT-MPIO was detected as early as 15 minutes and optimal uptake time was 1 to 2 hours. Bars show mean ± SEM and * represents $P < .05$. Three independent experiments were performed and three images were used as quantification in each independent experiment.

FIGURE 3. A, Cytotoxicity of Dual-MPIO. All three cell lines were treated with different concentrations of DT-MPIO for 24 hours. Cell viability was measured using the MTT assay. Data for surviving cells expressed as a percent of reference control (Ref) which is the cells without treatment of TNFα and MPIO. Results are expressed as means ± SEM of three independent experiments. B, In vivo biodistribution of DT-MPIO. Changes in the iron levels were measured by magnetic particles, in different tissues ranging from 30 minutes to 72 hours following administration of DT-MPIO. Results are expressed as means ± SEM of three independent experiments. C, Changes in blood

clearance of iron-oxide particles at different time points after administration of MPIO. Curve is fitted as one phase exponential decay (n =3).

FIGURE 4. Dual-MPIO uptake in aortic root after in vivo injection. A, Representative images of aortic root of *ApoE*$^{-/-}$ mice with atherogenic diet following in vivo injection of fluorescent-labelled DT-MPIO or IgG-MPIO, stained with Oil Red-O stain for lipids (ORO; positive area in red) and probed with antibodies of VCAM-1, P-selectin, MOMA2 (macrophage), CD31 (endothelial cell) and α-SMA (smooth muscle cells). Scale bars = 100 μm. MPIO staining, representing iron particles could be detected in atherosclerotic plaque as green fluorescence at the first 30 minutes and persisted up to 2 hours as compared to the controls (no DT-MPIO injection and IgG-MPIO injection). B, Percentage area of MPIO fluorescence signal in aortic root increased with in vivo MPIO circulation time in the mice (n = 4). C, Ex vivo MRI of aortic root following in vivo administration of DT-MPIO for 30 minutes. Dark spots were detected in the aortic root using DT-MPIO (n = 4) while no hypointensity could be detected that using control IgG-MPIO (n = 2) as shown in the higher magnification. Perls' stain confirmed the binding of iron particles (blue) to the plaques in aortic root.

FIGURE 5. Detection of atherosclerotic plaques by in vivo MRI following administration of Dual-MPIO. A, In vivo MRI of aortic root at different time-points following administration of DT-MPIO. Hypointensity signal in aortic root was detected within 2 hours. Change in mean SNR increased with time (n = 12). B, In vivo MRI and histology of aortic root. Histology of aortic root was performed after the 2-hour MRI

session. The change in hypointensity MR signal in DT-MPIO group was confirmed by the presence of green fluorescence-labelled MPIO in histology.

FIGURE 6. Relationship between inflammatory markers and the magnitude of signal change in MRI. A, Sample characteristics by contrast groups: No difference was observed in the mean VCAM-1, P-selectin or macrophages values in the two contrast groups ($P = 0.936$, $P = 0.817$ and $P = 0.564$, respectively). B, Mean (and 95% confidence interval) of signal change and Iron under DT-MPIO and IgG-MPIO: Both signal change and iron were significantly higher in DT-MPIO group than IgG-MPIO group. C-E, Correlation between signal change and inflammatory markers C: VCAM-1; D: P-selectin; E: macrophage by contrast groups.

FIGURE 7. Detection of asymptomatic plaques by Dual-MPIO in atherosclerotic mice using a cuff. A, In vivo MRI and histology of carotid artery. Cuff was implanted in RCCA to create stable plaque in OSS, atheroprotective plaque in HSS and unstable plaque in LSS region while the LCCA remained untreated as control. Hypointensity signal was observed in the MR images in the LSS region of RCCA. Histology confirmed that the plaques in the LSS are of vulnerable phenotype, characterized by high macrophage burden, thin cap of smooth muscle cells (α-SMC) and collagen (connective tissue), were targeted by DT-MPIO (Perl's stain). No hypointensity signal was observed in OSS region in MR images. Histology confirmed that minimal DT-MPIO binding to plaques in OSS region, which have stable phenotype with little macrophage, thick cap of smooth muscle cells and collagen. B, Highest mRNA levels of VCAM-1, P-selectin and

613 MIP-3 were detected in the region of LSS, followed by OSS and then HSS of the RCCA,
614 indicating that lesion at LSS region was more inflamed than those in OSS or HSS regions
615 (n = 3). C, Protein levels of VCAM-1, P-selectin and MIP-3 were consistent with mRNA
616 levels (n = 3).
617
618

SUPPLEMENTARY MATERIALS

MATERIALS AND METHODS

Synthesis of Fluorescent-Labelled Dual-ligand Microparticles of Iron Oxide (MPIO)

MPIO (1 μm diameter; Dynabeads® MyOneTM; Invitrogen) with p-toluenesulphonyl (tosyl) reactive surface groups were used for conjugation of antibody. To prepare fluorescent-labelled dual-targeted MPIO (DT-MPIO), 20 μg of purified monoclonal rat anti-mouse antibody for VCAM-1 (BD Biosciences), 20 μg of purified monoclonal mouse anti-mouse antibody for P-selectin (Santa Cruz Biotechnology) and 1 μg of fluorescein cadeverine (Molecular Probes), were covalently conjugated to 1 mg MPIO, by incubation at 37°C for 24 hours, with constant rotation. Control IgG-MPIO and single-targeted MPIO were conjugated with antibody for either IgG-1 (monoclonal rat anti-mouse antibodies for IgG-1; AbD Serotec), VCAM-1 or P-selectin. MPIO were then washed thrice in phosphate buffered saline (PBS) containing 0.1% bovine serum albumin (BSA) at 4°C and incubated with tris buffer (0.1 mol/L, 0.1% BSA, pH 7.4) at 37°C overnight, to block remaining active tosyl sites. MPIO were rinsed in PBS (0.1% BSA) at 4°C for 5 minutes and stored at 100 mg MPIO per mL PBS (0.1% BSA, 0.05% Tween and 0.02% sodium azide) at 4°C.

Cell culture

Mouse endothelial cells (C166, ATCC) and mouse macrophage (RAW 264, ATCC) were cultured in Dulbecco's Modified Eagle's Medium (DMEM) supplemented with 10% fetal bovine serum (FBS) and 1% antibiotic-antimycotic (Gibco). Mouse aorta smooth muscle cells (MOVAS, ATCC) were cultured in DMEM supplemented with 10%

FBS, 1% antibiotic-antimycotic (Gibco) and 0.2 mg/mL G-418 (Gibco).

In Vitro Dual-targeted MPIO Binding to TNFα Stimulated Cells

Mouse endothelial cells (C166, ATCC) and mouse macrophage (RAW 264, ATCC), mouse aorta smooth muscle cells (MOVAS, ATCC) were cultured in 15 cm culture dish with coverslips. They were incubated with different doses (0, 0.1, 1, 10 and 100 ng/mL) of murine recombinant tumour necrosis factor- α (TNFα) (Sigma) for 24 hours at 37°C to induce inflammation and expression of VCAM-1 and P-selectin. Prior to addition of MPIO, coverslips in each culture dish were taken out for the determination of VCAM-1 and P-selectin expression by immunocytochemistry. Remaining stimulated cells in dish were then incubated either with VCAM-1-MPIO (V-MPIO), P-selectin-MPIO (P-MPIO), dual-targeted MPIO (DT-MPIO) or IgG-MPIO (2 mg per 3 x 10^6 cells, 15 cm culture dish) for 1 hour at 37°C. Repeated rinses with phosphate-buffered saline (PBS) were performed to remove unbound MPIO. Cell bound-MPIO was directly observed under fluorescence microscope and its area per cell were quantified using public domain software, ImageJ. 3 independent experiments were performed.

For time-point experiment, the cells were incubated with 10 ng/mL TNFα for 24 hours at 37°C followed by DT-MPIO incubation for different time period (0, 15, 30, 60, 120 and 240 minutes). For blocking experiment, the target sites, i.e. VCAM-1 and P-selectin, expressed on TNFα treated cells (10 ng/mL) were initially blocked by single or both primary antibodies (anti-VCAM-1 and anti-P-selectin) before incubation with DT-MPIO. Area of cell bound-MPIO per cell was assessed as described above. 3 independent experiments were performed.

Immunocytochemistry

For immunostaining, TNFα treated cells on coverslips were fixed with 4% paraformaldehyde (PFA) for 15 minutes, permeabilized with 0.1% Triton X-100 for 5 minutes and blocked with 5% bovine serum albumin (BSA) for 30 minutes. Cells were then incubated with primary antibody against VCAM-1 (Rat anti-mouse, 1:200, BD Biosciences) and P-selectin (Mouse anti-mouse, 1:200, Santa Cruz Biotechnology) at room temperature for 1 hour, followed by secondary antibodies (Goat anti-rat DyLight 594, 1:200 and Rabbit anti-mouse DyLight 594, 1:200 respectively) for 30 minutes at room temperature. After repeated wash with PBS, coverslips were mounted on a slide in anti-fade reagent with DAPI (Molecular Probes). An Olympus IX-83 inverted microscope fitted with a 60×, 1.4 NA oil immersion objective (Olympus), and a monochrome CCD camera (Olympus) driven using CellSens (Olympus) were used. VCAM-1 and P-selectin fluorescence intensity per cell were quantified using ImageJ.

Cell growth and survival assay

MTT assay was conducted to assess cell survival and growth after addition of DT-MPIO. Endothelial cell lines were first stimulated by TNFα (10 ng/mL at 37°C for 24 hours) prior to incubation with different concentrations of DT-MPIO (0 – 2 mg/mL) for 24 hours. Reference control was also done with the cell line without stimulation of TNFα to eliminate the toxic effect of TNFα prior to addition of MPIO. MTT assay was conducted according to the manufacturer's manual (Cayman Chemical Company).

Biodistribution

For biodistribution, DT-MPIO were injected in vivo via tail vein (n = 3 *ApoE*$^{-/-}$ mice per group) and allowed to circulate for different time period (0, 0.5, 6, 24, 48, 72 hours). Mice were terminally anaesthetized. Lung, liver, spleen and kidney were collected and weighed before quantification of magnetic particles (Pepric, Belgium). Calibration was done by varying known MPIO amount (0-1 mg).

Immunohistochemistry of Aortic Root

At the end of MPIO circulation or imaging, mouse was sacrificed and the heart was excised. Upper part of heart was cut at the base of the aortic valves, embedded in Tissue Tek OCT (Optimal Cutting Temperature) compound (Miles Scientific) and stored at -80°C. Serial cryostat sections (6 μm thickness) were prepared on a cryostat, Reichert-Jung Cryocut 1800 (Leica Microsystems). To determine the distribution and localisation of MPIO in aortic root, serial sections underwent immunostaining for VCAM-1, P-selectin, endothelial cells (CD31; Abcam), macrophages (MOMA2; Abcam) and smooth muscle cells (αSMA; Abcam). Lipid staining by Oil Red O was used to visualize the lesion area.

Air-dried cryostat sections of aortic root were fixed with the pre-cooled acetone for 10 minutes at room temperature and rinsed with PBS three times. Non-specific staining was blocked by incubation with 3% BSA in PBS for 30 minutes and washed in PBS. Slides were then incubated with primary antibody in a 1:50 dilution at 4°C overnight, followed by secondary antibody in a 1:200 dilution of secondary antibodies for 1 hour at room temperature. Whole slide images were produced using Olympus IX-83 inverted

711 microscope as previously described. The histological staining in all images was
712 quantified in a standardised and objective way using ImageJ. The stained area of VCAM-
713 1, P-selectin, CD31, MOMA, αSMA and MPIO were quantified as a percentage of the
714 total aortic root area. The mean of stained area percentage in histological images from 3
715 sections per subject was calculated.
716
717 **Animals and In vivo Administration of Dual-MPIO**
718 All animal experiments were performed in accordance with UK Scientific Procedures
719 Act (1986) and local ethical approval. 70-week-old homozygous *ApoE*$^{-/-}$ mice were put
720 on a standard mouse chow diet until the day of experiment. DT-MPIO or control IgG-
721 MPIO were injected in vivo via the tail vein (5 mg iron per kg body weight in 150 μl PBS)
722 and allowed to circulate up to 2 hours (0, 0.5, 1, 1.5 and 2 hours). Mice were then
723 anaesthetized and underwent MRI scanning and/or histological analysis.
724
725 **Ex vivo in situ MRI following In Vivo Systemic Administration of Dual-Targeted**
726 **MPIO**
727 DT-MPIO (n = 4 mice) or control IgG-MPIO (n = 2 mice) (5 mg iron per kg body
728 weight in 150 μl PBS) was injected in vivo via tail vein and allowed to circulate for 30
729 minutes. *ApoE*$^{-/-}$ mice were sacrificed and perfusion fixed with 4% PFA.). Ex vivo in situ
730 MRI of aortic root was performed with a Direct Drive 9.4T Varian (Palo Alto, USA)
731 horizontal bore scanner with 100 G/cm gradients and bird cage radiofrequency coil
732 (RAPID biomedical GmbH, Germany) 33 mm internal diameter running VnmrJ 2.3A
733 software. A T2*-weighted 3-dimensional gradient echo sequence was used (TR: 40.00

ms; TE: 4.71 ms; FOV 25 x 25 x 25 mm; matrix size 256 x 256 x 128; average: 2; flip angle: 20°). The heart and aortic root were then removed en bloc for histology. Perls' stain was used to confirm the presence of MPIO binding to the atherosclerotic plaques in the aortic root**.**

In Vivo MRI of Aortic Root

The 70-week-old *ApoE*$^{-/-}$ mouse was anaesthetized and maintained with 1-2% isoflurane during imaging. MRI acquisition was both cardiac and respiratory gated. A Fast low angle shot (FLASH) sequence was used in baseline pre-contrast and post-contrast in vivo MRI of aortic root: TR: 22.2 ms; TE: 1.27 ms; FOV 25.6 x 25.6 mm; acquisition matrix: 256x256; average: 8; slice thickness: 0.5 mm; plane: axial; flip angle: 25°. DT-MPIO (n = 12 mice) or control IgG-MPIO (n = 7 mice) (5 mg iron per kg body weight in 150 μl PBS) was injected via the tail vein. Post-contrast in vivo MRI was performed from 20 minutes up to 2 hours after MPIO injection.

Quantitative MR Image Analysis of Aortic Root

Using the aortic valves as a reference marker, the inner and outer contours of the aortic root were delineated manually and independently by two observers and defined as the region of interest (ROI). The signal within the ROI (plaque signal) and that of a similar sized ROI in the background noise were measured using public domain software, ImageJ. The signal-to-noise ratio (SNR) of ROI was calculated:

SNR of ROI = (Signal within ROI) / (Signal in background noise)

The mean of SNR of all 3 consecutive slices per subject was calculated.

Implantation of Shear Stress Modifying Cuff in Carotid Arteries

The shear stress modifying cuff (provided by authors CM and KKB) and implantation procedure were described in previous studies.[13] The cone shaped inner lumen is imperative for creating defined regions of low (LSS, upstream), high (HSS, within the cuff) and oscillatory shear stress (OSS, downstream) within the common carotid artery (Figure 7).[13] At 18 weeks of age, the *ApoE*$^{-/-}$ mice were put on atherogenic diet 2 weeks prior to cuff implantation until the day of scanning. At week 20, surgical implantation of the shear stress modifying cuff was performed on one of the common carotid arteries (CCA) while the other CCA was left untreated as a control.

In vivo MRI of Carotid Arteries

At 29 weeks of age, i.e. 9 weeks post-collar placement, *ApoE*$^{-/-}$ mouse underwent in vivo MRI of carotid arteries. A 3-dimensional time of flight (TOF) angiography sequence, double gating, was used in baseline pre-contrast and post-contrast scanning: TR: 30.0 ms; TE: 1.20 ms; FOV 18x18x18 mm; acquisition matrix: 256x256x256; average: 2; slab thickness: 18mm; flip angle: 45°. Dual antibody-conjugated MPIO (n = 9 mice) or control IgG-1-MPIO (n = 5 mice) (5 mg iron per kg body weight in 150 μl PBS) was injected in vivo via tail vein. Post-contrast in vivo MRI was performed from 20 minutes up to 2 hours post-injection.

Histology of carotid arteries

At the end of the scanning session, *ApoE*$^{-/-}$ mouse was sacrificed, arterial tree was

perfusion fixed and the cuff was removed. To determine which phenotypes of carotid plaques targeted by dual-targeted MPIO, serial 4-μm-thick paraffin sections of the whole carotid artery across all three shear-stress regions underwent staining for iron (Perls') and connective tissue (Picrosirius Red), and immunostaining for macrophages (Mac-3), and smooth muscle cells [α smooth muscle actin (αSMA)]. Microscopy was performed.

mRNA Quantification in Carotid Artery by RT-PCR

The treated CCA of mice was divided into 3 regions, i.e. oscillatory shear stress (OSS), high shear stress (HSS) and low shear stress (LSS). Each region of 8 mice was collected into a tube for exaction of RNA, DNA and protein. 3 independent experiments were performed.

Total RNA from each region of carotid arteries were separately homogenized and extracted with the RNA/DNA/Protein kit (Invitrogen) according to the manufacturer's protocol. The concentration of total RNA was determined by Nanodrop ND-1000 Spectrophotometer (Thermo Fisher Scientific). cDNA synthesis was performed according to the protocol provided with M-MLV reverse transcriptase (Promega Corporation) using 200 units of enzyme, 0.5 μg of random primers (Invitrogen) as primers, and 1 μg of RNA. RT-PCR was carried out using aorta cDNA as template and analyzed in an ABI 7500 Fast Real-Time PCR Systems (Applied Biosystems). Real time PCR was performed to quantify mouse VCAM-1, P-selectin and macrophage inflammatory protein 3 (MIP3 or CCL20). mRNA Ct values for these genes were analyzed on SDS v1.4 Software (Applied Biosystems) and normalized to β-actin to generate a relative expression ratio. Oligonucleotides for RT-PCR were: VCAM-1: forward, 5′-

TGATTGGGAGAGACAAAGCA; reverse, 5′- GCAGCACACGTCAGAACAA; P-selectin: forward, 5′- AAGATGCCTGGCTACTGGACAC; reverse, 5′- CAAGAGGCTGAACGCAGGTCAT; CCL20: forward, 5′- TTTTGGGATGGAATTGGACAC; reverse, 5′- TGCAGGTGAAGCCTTCAACC; β-actin: forward, 5′-CATTGCTGACAGGATGCAGAAGG; reverse, 5′- TGCTGGAAGGTGGACAGTGAGG.

Protein Expression in Carotid Artery by Western Blotting

Protein lysates of each region of carotid arteries were isolated from the kit described above and were quantified by BCA protein assay kit (Pierce Biotechnology). Protein samples (30 μg) were separated by 12.5% SDS-PAGE and then transferred into nitrocellulose membranes (Bio-rad Laboratory). The membrane was blocked with 5% non-fat milk in Tris buffered saline (TBS)-Tween buffer and then probed overnight at 4°C with anti-VCAM-1 (1:1000), anti-P-selectin (1:1000), anti-MIP3 (1:1000, Abcam), anti-β-actin (1:2000, Cell Signaling Technology) It was followed by appropriate secondary antibodies conjugated to horseradish peroxidase for 1 hour with a 1:5000. After washing, the membrane was developed with enhanced chemiluminescence (ECL) kit (Amersham Pharmacia Biotechnology) and exposed to X-ray films (Amersham Pharmacia Biotechnology). Intensity of bands was quantified using ImageJ. Equal loading was corrected by β-actin immunoreactivity.

Statistical Analysis

Percent change of mean SNR signal, VCAM-1, P-selectin, macrophages and Iron were

summarised as mean (standard deviation) and compared between DT-MPIO and control IgG-MPIO using t-tests. The correlations between signal change and each of the other variables were estimated within each contrast group using Spearman's rank correlation coefficient (r). To assess whether the strength of the association between each of the biomarkers and signal change differed by contrast groups, linear models were used. Each model included the biomarker (where signal change was the outcome of interest) and contrast groups as main effects and an interaction between groups and biomarkers. The interaction term was used to determine whether the strength of the relationship differed between the contrast groups. The nature of the relationship between VCAM-1 and P-selectin and their effect on signal change under contrast groups was also explored by including an interaction between VCAM-1 and P-selectin. Intra-observer and inter-observer variability in measurement of percentage change of SNR in aortic vessel wall were analysed using Bland-Altman plot. All tests were two sided and $P < 0.05$ considered statistically significant. Analysis was conducted using Stata 13MP.